PHYSICAL REVIEW RESEARCH **4**, L032012 (2022)

Letter | Editors' Suggestion

Nanofocused x-ray photon correlation spectroscopy

Sharon Berkowicz,[1] Sudipta Das,[1] Mario Reiser,[1] Mariia Filianina,[1] Maddalena Bin,[1] Giulio Crevatin,[2] Franz Hennies,[3] Clemens Weninger,[3] Alexander Björling,[3] Paul Bell,[3] and Fivos Perakis[1,*]

[1]*Department of Physics, AlbaNova University Center, Stockholm University, SE-10691 Stockholm, Sweden*

[2]*Diamond Light Source, Harwell Science and Innovation Campus, Didcot, Oxfordshire OX11 0DE, United Kingdom*

[3]*MAX IV laboratory, Lund University, Lund 22100, Sweden*

(Received 17 December 2021; revised 19 May 2022; accepted 16 June 2022; published 25 July 2022)

Here, we demonstrate an experimental proof of concept for nanofocused x-ray photon correlation spectroscopy, a technique sensitive to nanoscale fluctuations present in a broad range of systems. The experiment, performed at the NanoMAX beamline at MAX IV, uses a novel event-based x-ray detector to capture nanoparticle structural dynamics with microsecond resolution. By varying the nanobeam size from $\sigma = 88$ nm to $\sigma = 2.5$ μm, we quantify the effect of the nanofocus on the small-angle scattering lineshape and on the diffusion coefficients obtained from nano-XPCS. We observe that the use of nanobeams leads to a multifold increase in speckle contrast, which greatly improves the experimental signal-to-noise ratio, quantified from the two-time intensity correlation functions. We conclude that it is possible to account for influence of the high beam divergence on the lineshape and measured dynamics by including a convolution with the nanobeam profile in the model.

DOI: 10.1103/PhysRevResearch.4.L032012

Diffraction-limited storage rings (DLSRs) exhibit unique properties due to the extremely low emittance, which allows us to create x-ray nanobeams that approach the diffraction-limit [1]. Facilitated by new technological advances, the realization of DLSRs has become possible in recent years, with MAX IV being the first fourth generation synchrotron light source to become operational. The unprecedentedly low emittance of DLSRs is enabled by the use of multibend achromat lattices, resulting in a substantial boost in x-ray brightness and transverse coherence compared with previous generation storage-rings [2]. In turn, this new capability opens up the field for a new class of experiments based on coherent x-ray techniques which benefit greatly from the increase of coherent flux [1].

X-ray photon correlation spectroscopy (XPCS) is an x-ray scattering technique that probes structural dynamics by utilizing the coherent properties of x-ray beams [3–7]. The dynamics are extracted by correlating the intensity in a time series of scattering images, which exhibit speckles due to the high degree of interference between the scattered x-ray waves. However, XPCS at third generation synchrotrons has been restricted to relatively slow dynamics occurring on timescales ranging from milliseconds to seconds [8–10], with limiting factors mainly being the detector frame-rate and the insufficient scattered intensity at the fastest accessible timescales. Recent advancement in detector technologies, in conjunction with higher coherent flux provided by the new DLSRs like MAX IV, allows for XPCS to be extended to the microsecond regime [6,11,12]. Event-driven detectors, such as those based on the Timepix3 chip, have no direct temporal limitation related to the frame-rate and offer XPCS access to dynamics on nanosecond timescales [13–15].

In principle, nanosized x-ray beams can advantageously be combined with XPCS into so-called nano-XPCS, and allow increased insight into nanoscale fluctuations present in a broad range of systems, such as liquid mixtures [16–18], biological solutions [19–21], metallic liquids [22,23], surface self-organization and island growth [24,25], stress relaxation [26] as well as in magnetic systems [27–29]. The spatial sensitivity to local dynamical information in heterogeneous samples could potentially also be maximized by combining nanobeams with x-ray compatible microfluidic sample environments [30]. Furthermore, the use of nanobeams can drastically increase the speckle size and contrast, thus opening the possibility for compact XPCS experiments at shorter sample-to-detector distances and at larger momentum transfer Q. The latter would in addition benefit particularly from combination with fast event-driven detectors due to the faster dynamics probed at larger Q, i.e., at smaller length scales.

Previous x-ray experiments have either studied static samples with nanobeams [31–33] or probed dynamics with significantly larger micron-sized beams [6,11,12]. Even though previous numerical simulations estimate the impact of the use of nanobeams for measuring dynamics [34], these predictions have not hitherto been verified experimentally due to several obstacles when it comes to this approach. These are related to the high beam divergence required for the nanofocus geometry, the limitations in coherent flux, as well as possible sample

*f.perakis@fysik.su.se

Published by the American Physical Society under the terms of the Creative Commons Attribution 4.0 International license. Further distribution of this work must maintain attribution to the author(s) and the published article's title, journal citation, and DOI.

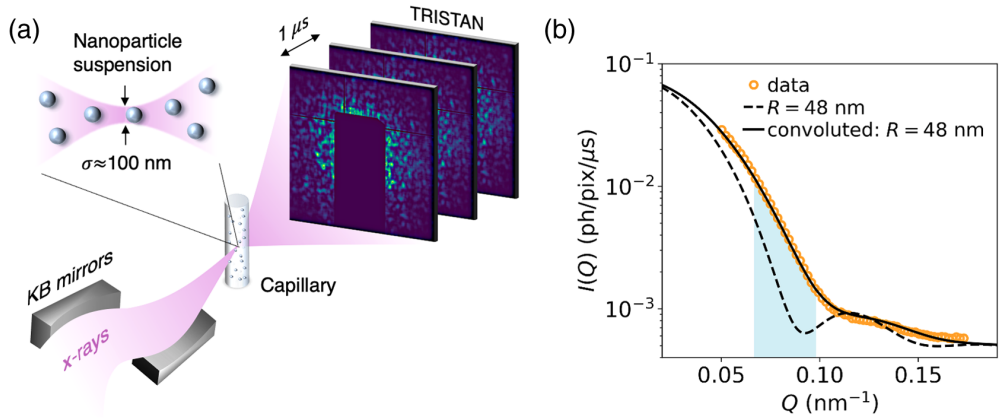

FIG. 1. (a) An illustration of the experimental scheme: The beam is focused using nanofocusing Kirkpatrick-Baez (KB) mirrors on the sample, consisting of nanoparticle suspensions in capillaries. The scattering data are recorded with the Tristan detector, reaching readout rates down to 1 μs. The direct beam is blocked by a beamblocker, indicated by the dark region in the center of the detector. (b) The angularly integrated small-angle x-ray scattering (SAXS) intensity for silica nanoparticles in pure water measured with beam size $\sigma = 88$ nm. Open circles denote experimental data while the lines refer to the model with the convolution of the beam profile (solid line) and without the convolution (dashed line) for particles with radius $R = 48$ nm.

and optics instabilities that can influence the extracted signal [31].

Here, we demonstrate a proof of concept for nano-XPCS by utilizing the coherent x-rays of MAX IV. By the use of x-ray nanobeams at the NanoMAX beamline [35,36], combined with the state-of-the-art event-based Tristan detector [13–15], we are able to resolve the dynamics of nanoparticle suspensions with microsecond resolution. Moreover, by varying the beam size from $\sigma = 88$ nm to $\sigma = 2.5$ μm, we compare the extracted temporal intensity autocorrelation (g_2) function obtained from nano-XPCS with that from micron-sized focus XPCS. We demonstrate that the use of nanobeams leads to multifold increase in the speckle contrast, which enhances the resolution and signal-to-noise (SNR) of the experiment, quantified from the two-time correlation (TTC) functions. Even though the measured g_2 relaxation times are influenced by the nanobeam divergence, we show that it is possible to account for this effect and recover the diffusion coefficient independent of the beam size.

A schematic of the experiment is illustrated in Fig. 1(a). XPCS measurements were carried out using a nanofocused x-ray beam in SAXS geometry at photon energy 10 keV, constant flux $\Phi = 1.5 \times 10^{10}$ s^{-1} and a sample-to-detector distance of 4 m, covering the momentum transfer Q range 0.05–0.18 nm^{-1}. Here, Q is defined as $Q = \frac{4\pi}{\lambda} \sin(\frac{\theta}{2})$, where λ is the x-ray wavelength and θ is the angle between the incident beam and the detector pixel. The samples consisted of dilute silica nanoparticle suspensions contained in 1-mm-diameter quartz capillaries. The nonfunctionalized silica nanoparticles were purchased from nanoComposix with 49-nm radius (estimated from TEM) and dispersed in two different solvents; in pure milli-Q water (0.48 vol% nanoparticles) and in a 33-mol% mixture of Dimethyl Sulfoxide (DMSO) and water (0.16 vol% nanoparticles). The x-ray beam was nanofocused using a pair of Kirkpatrick-Baez (KB) mirrors to a focal beam size $\sigma = 88$ nm (full-width half-maximum) with a beam divergence of 1.2 mrad, as described in more detail elsewhere [32]. To evaluate the effect of beam size, XPCS experiments were performed at three different sample positions along the beam path: the 1-mm-diameter sample capillary centered at the focus (beam size $\sigma = 88$ nm), 1 mm downstream ($\sigma = 1.3$ μm) and 2 mm downstream ($\sigma = 2.5$ μm) relative to the focus. It should be noted that since the edges of the capillary are ± 0.5 mm apart, the beam size within the sample varies with the beam divergence of 1.2 mrad, e.g., with the 88 nm focus in the center it increases to $\approx$700 nm at the edges.

Speckle patterns were recorded using a prototype Tristan detector from the Diamond Light Source, based on the Timepix3 chip [13,14]. The detector consists of 2069×515 pixels with a pixel size of 55×55 μm^2 with $\approx$1.5 ns nominal time resolution and 475 ns dead time per pixel. To acquire sufficient SNR, the individual pixels were binned to areas of 10×10 pixels, yielding photon count rates in the order of 10^{-3}–10^{-2} μs^{-1} per bin.

Figure 1(b) shows the angularly averaged SAXS intensity of the silica nanoparticles in pure water. To fit the SAXS lineshape we include in the model a convolution of the scattered intensity, derived from the particle form factor $|F(Q,R)|$, with the beam profile. This approach has been used previously for beams with high divergence, where a convolution with the point spread function (i.e., the beam profile) has been shown to affect the extracted lineshape [33,37]. Specifically, the angularly averaged SAXS intensity I is given by

$$I = I_0 * h, \tag{1}$$

where $I_0 \propto |F(Q,R)|^2$ is the theoretical intensity and the point spread function h is described by a model of the beam profile in the detector plane (see Supplemental Material [38], Fig. S2). In the Supplemental Material [38] (see Sec. S1) we have additionally included a simulation that validates the above approximation to convolute sample and beam intensities, rather than more complex calculations involving amplitudes, for estimating the smearing effect of the nanobeam divergence.

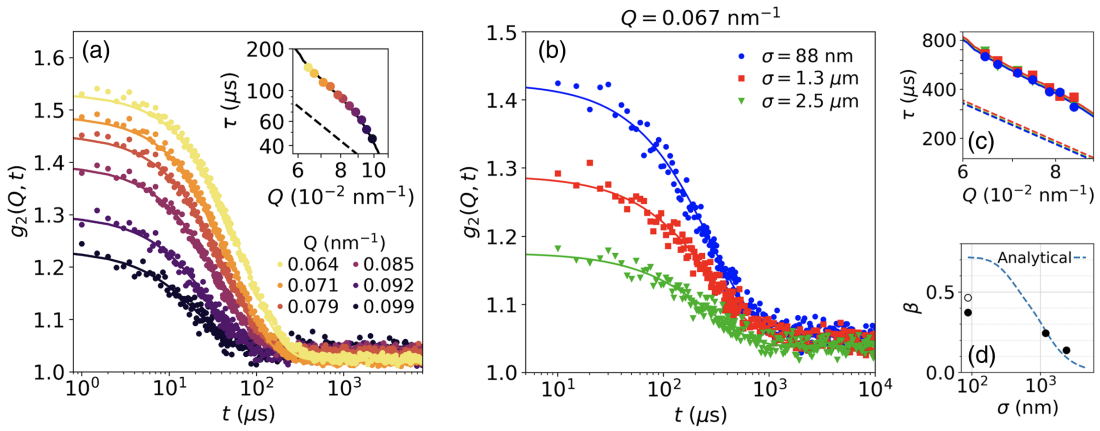

FIG. 2. (a) Intensity autocorrelation (g_2) functions at different Q for silica nanoparticles in pure water measured at the beam focus ($\sigma = 88$ nm). The inset shows the Q dependence of the average relaxation times τ obtained from fits of the g_2 functions to Eq. (3). The solid line denotes a fit to a model that incorporates a convolution with the divergent beam profile, while the dashed line represents the model in absence of the convolution. (b) g_2 functions for silica nanoparticles in DMSO-water solution measured at different beam sizes ($Q = 0.067$ nm^{-1}). (c) The Q dependence of the average relaxation times τ obtained from fits of the g_2 functions in panel (b) to Eq. (3). (d) Speckle contrast β versus beam size σ. The experimental β values from silica nanoparticles in water (open black circle) and DMSO-water (black circles), extracted from the fits to the g_2 functions ($Q = 0.067$ nm^{-1}) are compared with an analytical estimate (dashed line).

We find that the experimental data (orange open circles) overall show good agreement with the model (black solid line) based on a Schulz distribution, commonly used to describe particle size distributions [39,40], for spherical particles with fitted mean radius $R = 48$ nm and polydispersity $\Delta R/R \approx 8\%$ (standard deviation of the size distribution). For comparison, Fig. 1(b) additionally shows the scattered intensity calculated from the particle form factor without the convolution (dashed line) that would result from a low-divergence beam. The difference between the two lineshapes is striking and highlights the effect of the divergent nanobeam on SAXS measurements. In particular, the beam divergence causes a smearing out of the scattered intensity lineshape towards larger momentum transfer Q, consistent with previous observations [33]. The blue-shaded region indicates the momentum transfer range $Q \approx 0.06$–0.10 nm^{-1} where the XPCS analysis is performed.

The nanoparticle dynamics were analyzed by calculating the temporal intensity autocorrelation (g_2) function, which is defined as [41]

$$g_2(Q,t) = \frac{\langle I(Q,t_0)I(Q,t_0+t)\rangle}{\langle I(Q,t_0)\rangle^2}, \tag{2}$$

where $I(Q,t_0)$ and $I(Q,t_0+t)$ denote the intensity of a pixel at time t_0 and after delay time t, respectively. The bracket notation refers to averaging over time t_0 and pixels that belong to a given Q bin, i.e., a thin radial slice around the beam center corresponding to vector values $\mathbf{Q}$ in a frame of scattered intensity. The g_2 functions are fit to single exponential functions of the form

$$g_2(Q,t) = \beta \exp(-2t/\tau) + c, \tag{3}$$

where τ is the relaxation time, β is the speckle contrast which depends on experimental parameters, such as the coherence of the x-ray beam [42], and c is the offset.

Figure 2(a) shows the intensity autocorrelation functions (g_2) of nanoparticles in pure water measured in the beam focal plane ($\sigma = 88$ nm) at different momentum transfer values Q. The relaxation times τ exhibit a Q dependence, as shown in the inset. To recover accurate diffusion coefficients, one needs to fit a model that incorporates the convolution of the relaxation times with the beam profile, due to the large beam divergence of 1.2 mrad. In particular, the experimental relaxation times are obtained by convoluting the theoretical relaxation times τ_0, weighted by the theoretical intensity I_0, with the point-spread function h (see Supplemental Material [38], Sec. S1):

$$\tau = (\tau_0 I_0) * h/(I_0 * h). \tag{4}$$

For simple diffusion, the theoretical relaxation time is given by $\tau_0^{-1} = DQ^2$, where D is the translational diffusion coefficient. We find that such a model can accurately reproduce the experimental results, as indicated in the insets (solid line), and can account for the measured relaxation times and the deviation from the typical diffusive behavior $\tau^{-1} \propto Q^2$, contrary to the analysis without the convolution (dashed line).

From the fitted diffusion coefficient in water, $D = (3.6 \pm 0.1)$ nm$^2/\mu$s, we further calculate the hydrodynamic radius R_h based on the known solvent viscosity η and temperature T by the *Stokes-Einstein relation* [43],

$$D = \frac{k_B T}{6\pi R_h \eta}, \tag{5}$$

Using the viscosity of water at room temperature, we determine the hydrodynamic radius for the nanoparticles in pure water to $R_h = 62 \pm 1$ nm, which is larger than the radius extracted from SAXS [see Fig. 1(b)]. It is possible that the SAXS lineshape is less sensitive to the presence of nanoparticle aggregates than the dynamics extracted from XPCS analysis, which could explain the difference between R (SAXS) and R_h (XPCS). The deduced value of R_h is consistent with the hydrodynamic radius $R_h = 63 \pm 1$ nm measured from dynamic light scattering (see Supplemental Material [38], Sec. S2).

Furthermore, we investigate the effect of beam size on the measured nanoparticle dynamics. Figure 2(b) displays the intensity autocorrelation (g_2) functions ($Q = 0.067$ nm^{-1}) for silica nanoparticles suspended in a 33-mol% DMSO-water mixture for varying beam sizes, $\sigma = 88$ nm (in the focal plane), $\sigma = 1.3$ μm and $\sigma = 2.5$ μm, which correspond to different sample positions along the nanofocused beam. Here, we observe that the nanobeam leads to a substantial increase in the speckle contrast in comparison with micron-sized focus, and increases from $\beta = 0.12$ for $\sigma = 2.5$ μm to $\beta = 0.36$ for $\sigma = 88$ nm. This effect is attributed to the size ratio of the speckles S and the binned detector pixels P, since the speckle size is inversely proportional to the beam size σ by $S = \lambda L/\sigma$, where L is the sample-to-detector distance and λ is the x-ray wavelength [44]. For nanobeam sizes, we are in the regime where $S/P > 1$, which can explain the increase in contrast.

It is possible to analytically estimate the expected speckle contrast based on x-ray optics calculations [42,44]. Here, we compare the experimental contrast with an analytical estimate using the formalism in Refs. [44,45] for the experimental conditions used (see Supplemental Material [38], Sec. S3). The transverse coherence length ϵ in the sample planes used in the analytical contrast calculations was estimated based on the divergence α and x-ray wavelength λ by $\epsilon = \lambda/\alpha$ [46,47]. The estimated contrast as a function of beam size is shown in Fig. 2(d). We observe that the multifold contrast increase is also reproduced theoretically in qualitative agreement with the experimental data. The observed deviation of the experimental contrast from the theoretical estimate (dashed line) for the smallest beam size (the sample centered at the focal plane) can be attributed to the high divergence and beam size variation along the optical axis. In particular, the analytical estimate does not directly include any effects due to the high beam divergence (except for averaging the varying beam sizes within the sample, see Supplemental Material [38], Eq. S.11) where, for instance, the theoretical formula relies on the Fraunhofer diffraction in the far-field limit. The influence of the nanobeam divergence and the beam size variation along the optical path are most pronounced when the sample is centered at the nanofocus (see Supplemental Material [38], Fig. S4), which can explain the discrepancy between the calculated and measured contrast. Reducing the sample thickness along the optical axis would likely minimize the discrepancy while at the same time maximize the measured contrast, along with increased spatial resolution.

Similar to the nanoparticle-water suspension discussed above [Fig. 2(a)], we determine the particle hydrodynamic radius of the nanoparticles in DMSO-water measured in the focal plane, using the Stokes-Einstein relation and the viscosity of the mixture at room temperature [48], which yields $R_h = 61 \pm 1$ nm, consistent with the measurements in pure water. As indicated in Fig. 2(c), we do not observe any significant variation of the relaxation times, nor of the normalized g_2 functions (see Supplemental Material [38], Sec. S4), as a function of the beam size. From the absence of beam size dependence in the measured dynamics, as well as in the SAXS profile (see Supplemental Material [38], Sec. S5), we exclude any significant influence from number density fluctuations (see Supplemental Material [38], Sec. S6) [49–51] and beam-induced effects [20,52,53], such as nanoparticle aggregation or heating due to the nanofocused beam.

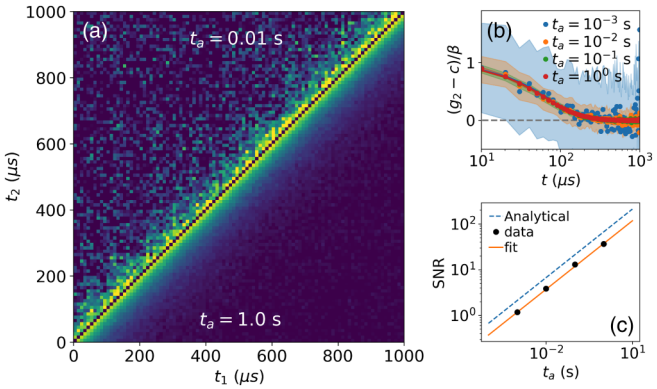

FIG. 3. (a) Two-time correlation (TTC) functions at $Q = 0.066$ nm^{-1} for silica nanoparticles in water at the beam focus ($\sigma = 88$ nm) averaged over an acquisition time (top) $t_a = 0.01$ s and (bottom) $t_a = 1$ s. (b) The average correlation function (g_2) obtained by averaging the antidiagonals of the TTC for various acquisition times t_a. The shaded areas denote the noise level. (c) Signal-to-noise ratio (SNR) of TTCs as a function of acquisition time. The experimental SNR (black dots) agrees with the analytical estimate (blue dashed line).

To investigate whether nano-XPCS can be used for probing heterogeneous dynamics and nanoscale fluctuations we calculate the TTC [54], which is defined as

$$c_2(Q, t_1, t_2) = \frac{\langle I(Q, t_1) I(Q, t_2) \rangle_{\text{pix}}}{\langle I(Q, t_1) \rangle_{\text{pix}} \langle I(Q, t_2) \rangle_{\text{pix}}}, \tag{6}$$

where $I(Q, t_1)$ and $I(Q, t_2)$ denote the intensity of a pixel at distinct times t_1 and t_2. The subscript "pix" implies that, contrary to the g_2 definition, the averaging is in this case solely performed over pixels and not over time.

Figure 3(a) shows the TTCs measured with nanoparticles in water at the focus position ($\sigma = 88$ nm) with 10 μs time resolution. For the corresponding TTCs in the DMSO-water solution we refer to Supplemental Material [38], Sec. S7. The extracted dynamics quantified by the TTC is consistent with the g_2 analysis, indicating that it is possible to accurately extract the TTC with nanofocused beams. The TTC was further evaluated by computing the average $\langle c_2 \rangle$ and the standard deviation (σ_{c_2}) from the antidiagonals that emanate from the main diagonal of the TTC, and by analyzing the SNR, β/σ_β, where β is the contrast, i.e., the initial value of $\langle c_2 \rangle/\sigma_{c_2}$. The SNR is improved by averaging several TTCs, as can be observed by comparison of the upper and lower half of Fig. 3(a), where the former is computed with an acquisition time of $t_a = 0.01$ s and the latter with $t_a = 1$ s. Here, we define the acquisition time as $t_a = N_{TTC} t_{fr}$, where N_{TTC} is the number of TTCs used for the averaging and t_{fr} is the single-frame exposure time. As the acquisition time increases, from $t_a = 1$ ms to $t_a = 1$ s, the SNR increases by $t_{fr}\sqrt{N_{TTC}}$ [see Fig. 3(b)]. Moreover, the experimental SNR in Fig. 3(b) (black dots) shows good agreement with the analytical estimation (blue dashed line) based on the contrast (β), average intensity per pixel per second (I_{pix}), number of pixels (N_{pix}) and the number of TTCs (N_{TTC}), where the SNR is given by

SNR $=\beta I_{\mathrm{pix}} t_{fr}\sqrt{N_{TTC} N_{\mathrm{pix}}}$ [8]. From the analysis of the TTC functions, one can conclude that sufficient SNR (SNR $>$ 10) for the studied system and experimental conditions is achieved for $t_a \geqslant 0.1$ s in the small-Q range in $Q = 0.06$–0.08 nm^{-1}.

In conclusion, we have demonstrated a proof of concept for nano-XPCS by utilizing the coherent x-ray properties at MAX IV. The experiment presented here is the first experimental demonstration of dynamic measurements using nanobeams, as previous experimental studies in the literature have used nanobeams for imaging applications of static samples [31–33]. The use of nanobeams results in a significant increase in the speckle contrast, which translates to a multifold improvement in the SNR. With state-of-the-art event-based Tristan x-ray detector, we are able to measure the dynamics of nanoparticle suspensions with microsecond resolution. Furthermore, we demonstrate how to solve the critical problem of nanobeam divergence and that it is feasible to recover the diffusion coefficients, thus obtaining nanoscale dynamic information with multifold increase in SNR and spatial sensitivity. Finally, by analyzing the TTC functions we quantify the SNR and provide analytical predictions for designing nano-XPCS experiments. The advantage of nanobeams for SNR improvements in XPCS measurements can be summarized as follows: reducing the size of the beam increases the size of the speckles. Large speckle size allows for shorter sample-to-detector distance, or alternatively, binning of pixels in the area detector, without significant loss of speckle resolution. This results in higher intensities measured in each speckle, which improves the statistics in estimating the time correlations. With a larger coherent beam, the increase of the number of independent speckles in the area detector cannot fully compensate for their lower intensity. In addition, the gain in speckle contrast from using nanobeams can be utilized to access dynamics by XPCS at larger momentum transfer Q, i.e., at smaller length scales, which at the same time minimizes the influence of the nanobeam divergence, as would be important for more complex sample systems.

These experimental results demonstrate that coherent nanobeams can be used to enhance sensitivity to nanoscale fluctuations, present in a broad range of systems across fields, by combining structural information obtained from nanobeam x-ray scattering with dynamic content acquired from correlation analysis. Moreover, the combination of nanobeams with increased resolution along the optical axis, by minimizing the sample thickness e.g., using x-ray compatible microfluidic sample environments [30], could unlock the full potential for locally probing spatially heterogeneous dynamics with nano-XPCS.

The datasets generated during and/or analyzed during the current study are openly available in the figshare repository with [55].

The authors acknowledge MAX IV Laboratory for time on Beamline NanoMAX under Proposal 20200130. Research conducted at MAX IV, a Swedish national user facility, is supported by the Swedish Research council under contract 2018-07152, the Swedish Governmental Agency for Innovation Systems under contract 2018-04969 and Formas under contract 2019-02496. We acknowledge financial support by the Swedish National Research Council (Vetenskapsrådet) under Grant No.2019-05542 and within the Röntgen-Ångström Cluster Grant No. 2019-06075. This research is supported by Center of Molecular Water Science (CMWS) of DESY in an Early Science Project, the MaxWater initiative of the Max-Planck-Gesellschaft and the Wenner-Gren Foundations.

[1] R. Hettel, DLSR design and plans: an international overview, J. Synchrotron Radiat. **21**, 843 (2014).

[2] P. F. Tavares, S. C. Leemann, M. Sjöström, and Å. Andersson, The MAX IV storage ring project, J. Synchrotron Radiat. **21**, 862 (2014).

[3] G. Grübel, A. Madsen, and A. Robert, X-ray photon correlation spectroscopy (XPCS), in *Soft Matter Characterization* (Springer Science+Business Media, LLC, New York, 2008), pp. 953–995.

[4] A. Madsen, A. Fluerasu, and B. Ruta, Structural dynamics of materials probed by X-ray photon correlation spectroscopy, in *Synchrotron Light Sources and Free-Electron Lasers: Accelerator Physics, Instrumentation and Science Applications* (Springer International Publishing, Switzerland, 2016), pp. 1617–1641.

[5] O. G. Shpyrko, X-ray photon correlation spectroscopy, J. Synchrotron Radiat. **21**, 1057 (2014).

[6] A. R. Sandy, Q. Zhang, and L. B. Lurio, Hard X-ray photon correlation spectroscopy methods for materials studies, Annu. Rev. Mater. Res. **48**, 167 (2018).

[7] S. K. Sinha, Z. Jiang, and L. B. Lurio, X-ray photon correlation spectroscopy studies of surfaces and thin films, Adv. Mater. **26**, 7764 (2014).

[8] F. Perakis and C. Gutt, Towards molecular movies with X-ray photon correlation spectroscopy, Phys. Chem. Chem. Phys. **22**, 19443 (2020).

[9] Q. Zhang, E. M. Dufresne, and A. R. Sandy, Dynamics in hard condensed matter probed by X-ray photon correlation spectroscopy: present and beyond, Curr. Opin. Solid State Mater. Sci. **22**, 202 (2018).

[10] F. Lehmkühler, W. Roseker, and G. Grübel, From femtoseconds to hours—measuring dynamics over 18 orders of magnitude with coherent X-rays, Appl. Sci. **11**, 6179 (2021).

[11] Q. Zhang, E. M. Dufresne, S. Narayanan, P. Maj, A. Koziol, R. Szczygiel, P. Grybos, M. Sutton, and A. R. Sandy, Sub-microsecond-resolved multi-speckle X-ray photon correlation spectroscopy with a pixel array detector, J. Synchrotron Radiat. **25**, 1408 (2018).

[12] Q. Zhang, E. M. Dufresne, Y. Nakaye, P. R. Jemian, T. Sakumura, Y. Sakuma, J. D. Ferrara, P. Maj, A. Hassan, D. Bahadur, S. Ramakrishnan, F. Khan, S. Veseli, A. R. Sandy, N. Schwarz, and S. Narayanan, 20 μs-resolved high-throughput X-ray photon correlation spectroscopy on a 500k pixel detector enabled by data-management workflow, J. Synchrotron Radiat. **28**, 259 (2021).

[13] T. Poikela, J. Plosila, T. Westerlund, M. Campbell, M. De Gaspari, X. Llopart, V. Gromov, R. Kluit, M. van Beuzekom, F. Zappon, V. Zivkovic, C. Brezina, K. Desch, Y. Fu, and A. Kruth, Timepix3: A 65k channel hybrid pixel readout chip with simultaneous toa/tot and sparse readout, J. Instrum. **9**, C05013 (2014).

[14] H. Yousef, G. Crevatin, E. N. Gimenez, I. Horswell, D. Omar, and N. Tartoni, Timepix3 as x-ray detector for time resolved synchrotron experiments, Nucl. Instrum. Methods Phys. Res., Sect. A **845**, 639 (2017).

[15] A. S. Tremsin, J. V. Vallerga, O. H. W. Siegmund, J. Woods, L. E. De Long, J. T. Hastings, R. J. Koch, S. A. Morley, Y.-D. Chuang, and S. Roy, Photon-counting MCP/Timepix detectors for soft X-ray imaging and spectroscopic applications, J. Synchrotron Radiat. **28**, 1069 (2021).

[16] F. Perakis, K. Amann-Winkel, F. Lehmkühler, M. Sprung, D. Mariedahl, J. A. Sellberg, H. Pathak, A. Späh, F. Cavalca, D. Schlesinger, A. Ricci, A. Jain, B. Massani, F. Aubree, C. J. Benmore, T. Loerting, G. Gröbel, L. G. Pettersson, and A. Nilsson, Diffusive dynamics during the high-to-low density transition in amorphous ice, Proc. Natl. Acad. Sci. USA **114**, 8193 (2017).

[17] K.-I. Oh and C. R. Baiz, Molecular heterogeneity in aqueous cosolvent systems, J. Chem. Phys. **152**, 190901 (2020).

[18] D. Sheyfer, Q. Zhang, J. Lal, T. Loeffler, E. Dufresne, A. Sandy, S. Narayanan, S. Sankaranarayanan, R. Szczygiel, P. Maj, L. Soderholm, M. Antonio, and G. Stephenson, Nanoscale Critical Phenomena in a Complex Fluid Studied by X-Ray Photon Correlation Spectroscopy, Phys. Rev. Lett. **125**, 125504 (2020).

[19] Y. Shin and C. P. Brangwynne, Liquid phase condensation in cell physiology and disease, Science **357**, eaaf4382 (2017).

[20] N. Begam, A. Ragulskaya, A. Girelli, H. Rahmann, S. Chandran, F. Westermeier, M. Reiser, M. Sprung, F. Zhang, C. Gutt, and F. Schreiber, Kinetics of Network Formation and Heterogeneous Dynamics of an Egg White Gel Revealed by Coherent X-Ray Scattering, Phys. Rev. Lett. **126**, 098001 (2021).

[21] A. Girelli, H. Rahmann, N. Begam, A. Ragulskaya, M. Reiser, S. Chandran, F. Westermeier, M. Sprung, F. Zhang, C. Gutt, and F. Schreiber, Microscopic Dynamics of Liquid-Liquid Phase Separation and Domain Coarsening in a Protein Solution Revealed by X-Ray Photon Correlation Spectroscopy, Phys. Rev. Lett. **126**, 138004 (2021).

[22] B. Ruta, Y. Chushkin, G. Monaco, L. Cipelletti, E. Pineda, P. Bruna, V. M. Giordano, and M. Gonzalez-Silveira, Atomic-Scale Relaxation Dynamics and Aging in a Metallic Glass Probed by X-Ray Photon Correlation Spectroscopy, Phys. Rev. Lett. **109**, 165701 (2012).

[23] B. Ruta, S. Hechler, N. Neuber, D. Orsi, L. Cristofolini, O. Gross, B. Bochtler, M. Frey, A. Kuball, S. Riegler, M. Stolpe, Z. Evenson, C. Gutt, F. Westermeier, R. Busch, and I. Gallino, Wave-Vector Dependence of the Dynamics in Supercooled Metallic Liquids, Phys. Rev. Lett. **125**, 055701 (2020).

[24] P. Myint, K. F. Ludwig, L. Wiegart, Y. Zhang, A. Fluerasu, X. Zhang, and R. L. Headrick, de Gennes Narrowing and Relationship between Structure and Dynamics in Self-Organized Ion-Beam Nanopatterning, Phys. Rev. Lett. **126**, 016101 (2021).

[25] G. Ju, D. Xu, M. J. Highland, C. Thompson, H. Zhou, J. A. Eastman, P. H. Fuoss, P. Zapol, H. Kim, and G. B. Stephenson, Coherent x-ray spectroscopy reveals the persistence of island arrangements during layer-by-layer growth, Nat. Phys. **15**, 589 (2019).

[26] F. Dallari, A. Martinelli, F. Caporaletti, M. Sprung, G. Grübel, and G. Monaco, Microscopic pathways for stress relaxation in repulsive colloidal glasses, Sci. Adv. **6**, eaaz2982 (2020).

[27] S. Gorfman, A. A. Bokov, A. Davtyan, M. Reiser, Y. Xie, Z.-G. Ye, A. V. Zozulya, M. Sprung, U. Pietsch, and C. Gutt, Ferroelectric domain wall dynamics characterized with x-ray photon correlation spectroscopy, Proc. Natl. Acad. Sci. USA **115**, E6680 (2018).

[28] O. G. Shpyrko, E. D. Isaacs, J. M. Logan, Y. Feng, G. Aeppli, R. Jaramillo, H. C. Kim, T. F. Rosenbaum, P. Zschack, M. Sprung, S. Narayanan, and A. R. Sandy, Direct measurement of antiferromagnetic domain fluctuations, Nature (London) **447**, 68 (2007).

[29] X. M. Chen, B. Farmer, J. S. Woods, S. Dhuey, W. Hu, C. Mazzoli, S. B. Wilkins, R. V. Chopdekar, A. Scholl, I. K. Robinson, L. E. De Long, S. Roy, and J. T. Hastings, Spontaneous Magnetic Superdomain Wall Fluctuations in an Artificial Antiferromagnet, Phys. Rev. Lett. **123**, 197202 (2019).

[30] A. Ghazal, J. P. Lafleur, K. Mortensen, J. P. Kutter, L. Arleth, and G. V. Jensen, Recent advances in x-ray compatible microfluidics for applications in soft materials and life sciences, Lab Chip **16**, 4263 (2016).

[31] A. Björling, L. A. B. Marçal, J. Solla-Gullón, J. Wallentin, D. Carbone, and F. R. N. C. Maia, Three-Dimensional Coherent Bragg Imaging of Rotating Nanoparticles, Phys. Rev. Lett. **125**, 246101 (2020).

[32] L. Chayanun, L. Hrachowina, A. Björling, M. T. Borgström, and J. Wallentin, Direct three-dimensional imaging of an x-ray nanofocus using a single 60 nm diameter nanowire device, Nano Lett. **20**, 8326 (2020).

[33] K. Kawahara, K. Gohara, Y. Maehara, T. Dobashi, and O. Kamimura, Beam-divergence deconvolution for diffractive imaging, Phys. Rev. B **81**, 081404(R) (2010).

[34] O. Bikondoa and D. Carbone, X-ray photon correlation spectroscopy with coherent nanobeams: A numerical study, Crystals **10**, 766 (2020).

[35] U. Johansson, D. Carbone, S. Kalbfleisch, A. Björling, M. Kahnt, S. Sala, T. Stankevic, M. Liebi, A. Rodriguez Fernandez, B. Bring, D. Paterson, K. Thånell, P. Bell, D. Erb, C. Weninger, Z. Matej, L. Roslund, K. Åhnberg, B. Norsk Jensen, H. Tarawneh *et al.*, Nanomax: the hard x-ray nanoprobe beamline at the MAX IV Laboratory, J. Synchrotron Radiat. **28**, 1935 (2021).

[36] A. Björling, S. Kalbfleisch, M. Kahnt, S. Sala, K. Parfeniukas, U. Vogt, D. Carbone, and U. Johansson, Ptychographic characterization of a coherent nanofocused x-ray beam, Opt. Express **28**, 5069 (2020).

[37] Y. Sasanuma, R. V. Law, Y. Kobayashi, and K. Sasaki, Small-angle x-ray scattering measurements and image reconstruction by the maximum entropy method, Anal. Chem. **69**, 794 (1997).

[38] See Supplemental Material at http://link.aps.org/supplemental/10.1103/PhysRevResearch.4.L032012 for details on data analysis, analytical estimations and simulations, as well as for additional data and data representations.

[39] J. Als-Nielsen and D. McMorrow, Kinematical scattering I: Non-crystalline materials, in *Elements of Modern X-ray Physics*,

1st ed. (John Wiley & Sons, United Kingdom, 2011), pp. 113–146.

[40] S. R. Aragón, Theory of dynamic light scattering from polydisperse systems, J. Chem. Phys. **64**, 2395 (1976).

[41] B. J. Berne and R. Pecora, *Dynamic Light Scattering: With Applications to Chemistry, Biology, and Physics*, 2nd ed. (Dover Publications, Mineola, New York, 2000).

[42] S. O. Hruszkewycz, M. Sutton, P. H. Fuoss, B. Adams, S. Rosenkranz, K. F. Ludwig, W. Roseker, D. Fritz, M. Cammarata, D. Zhu, S. Lee, H. Lemke, C. Gutt, A. Robert, G. Grübel, and G. B. Stephenson, High Contrast X-ray Speckle from Atomic-Scale Order in Liquids and Glasses, Phys. Rev. Lett. **109**, 185502 (2012).

[43] A. Einstein, Über die von der molekularkinetischen theorie der wärme geforderte bewegung von in ruhenden flüssigkeiten suspendierten teilchen, Ann. Phys. (Berlin, Ger.) **322**, 549 (1905).

[44] J. Möller, M. Sprung, A. Madsen, and C. Gutt, X-ray photon correlation spectroscopy of protein dynamics at nearly diffraction-limited storage rings, IUCrJ **6**, 794 (2019).

[45] A. R. Sandy, L. B. Lurio, S. G. J. Mochrie, A. Malik, G. B. Stephenson, J. F. Pelletier, and M. Sutton, Design and characterization of an undulator beamline optimized for small-angle coherent x-ray scattering at the advanced photon source, J. Synchrotron Radiat. **6**, 1174 (1999).

[46] J. Als-Nielsen and D. McMorrow, X-rays and their interaction with matter, in *Elements of Modern X-ray Physics*, 1st ed. (John Wiley & Sons, Ltd, Chichester, West Sussex, UK, 2011), pp. 1–28.

[47] G. Ju, M. J. Highland, C. Thompson, J. A. Eastman, P. H. Fuoss, H. Zhou, R. Dejus, and G. B. Stephenson, Characterization of the x-ray coherence properties of an undulator beamline at the advanced photon source, J. Synchrotron Radiat. **25**, 1036 (2018).

[48] S. A. Schichman and R. L. Amey, Viscosity and local liquid structure in dimethyl sulfoxide-water mixtures, J. Phys. Chem. **75**, 98 (1971).

[49] H. Voigt and S. Hess, Comparison of the intensity correlation function and the intermediate scattering function of fluids: A molecular dynamics study of the Siegert relation, Phys. A (Amsterdam, Neth.) **202**, 145 (1994).

[50] S. R. Aragón and R. Pecora, Fluorescence correlation spectroscopy as a probe of molecular dynamics, J. Chem. Phys. **64**, 1791 (1976).

[51] Evelien J. Nijman, Henk G. Merkus, Jan C. M. Marijnissen, and Brian Scarlett, Simulations and experiments on number fluctuations in photon-correlation spectroscopy at low particle concentrations, Appl. Opt. **40**, 4058 (2001).

[52] F. Lehmkühler, F. Dallari, A. Jain, M. Sikorski, J. Möller, L. Frenzel, I. Lokteva, G. Mills, M. Walther, H. Sinn, F. Schulz, M. Dartsch, V. Markmann, R. Bean, Y. Kim, P. Vagovic, A. Madsen, A. P. Mancuso, and G. Grübel, Emergence of anomalous dynamics in soft matter probed at the European XFEL, Proc. Natl. Acad. Sci. USA **117**, 24110 (2020).

[53] B. Ruta, F. Zontone, Y. Chushkin, G. Baldi, G. Pintori, G. Monaco, B. Rufflé, and W. Kob, Hard x-rays as pump and probe of atomic motion in oxide glasses, Sci. Rep. **7**, 3962 (2017).

[54] A. Madsen, R. L. Leheny, H. Guo, M. Sprung, and O. Czakkel, Beyond simple exponential correlation functions and equilibrium dynamics in x-ray photon correlation spectroscopy, New J. Phys. **12**, 055001 (2010).

[55] DOI: 10.17045/sthlmuni.20198975.